ACS Energy LETTERS

Cite This: ACS Energy Lett. 2018, 3, 2059−2067

http://pubs.acs.org/journal/aelccp

LETTER

A Localized High-Concentration Electrolyte with Optimized Solvents and Lithium Difluoro(oxalate)borate Additive for Stable Lithium Metal Batteries

Lu Yu,[†] Shuru Chen,[†] Hongkyung Lee,[†] Linchao Zhang,[†,‡] Mark H. Engelhard,[§] Qiuyan Li,[†] Shuhong Jiao,[†] Jun Liu,[†] Wu Xu,*[,†] and Ji-Guang Zhang*[,†]

[†]Energy and Environment Directorate, Pacific Northwest National Laboratory, 902 Battelle Boulevard, Richland, Washington 99354, United States

[‡]Key Laboratory of Materials Physics, Institute of Solid State Physics, Chinese Academy of Sciences, Hefei, Anhui 230026, People's Republic of China

[§]Environmental Molecular Sciences Laboratory, Pacific Northwest National Laboratory, 3335 Innovation Boulevard, Richland, Washington 99354, United States

Supporting Information

ABSTRACT: We report a carbonate-based localized high-concentration electrolyte (LHCE) with a fluorinated ether as a diluent for 4-V class lithium metal batteries (LMBs), which enables dendrite-free Li deposition with a high Li Coulombic efficiency (~98.5%) and much better cycling stability for Li metal anodes than previously reported dimethyl carbonate-based LHCEs at lean electrolyte conditions. This electrolyte consists of 1.2 M lithium bis(fluorosulfonyl)-imide (LiFSI) in a cosolvent mixture of ethylene carbonate (EC)/ethyl methyl carbonate (EMC) with bis(2,2,2-trifluoroethyl) ether (BTFE) as the diluent and 0.15 M lithium difluoro(oxalate)borate (LiDFOB) as an additive. A Li||$LiNi_{1/3}Mn_{1/3}Co_{1/3}O_2$ battery with a high areal loading of 3.8 mAh cm^{-2} maintains 84% of its initial capacity after 100 cycles. The enhanced stability can be attributed to the robust solid−electrolyte interface (SEI) layer formed on the Li metal anode, arising from the preferential decomposition of LiDFOB salt and EC solvent molecules.

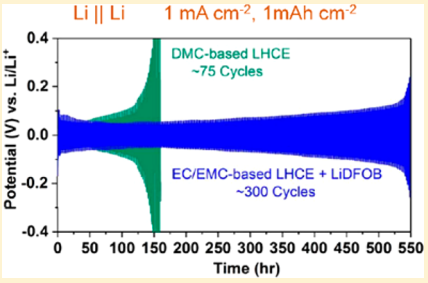

Development of high energy density batteries employing lithium (Li) metal as the anode is important to a variety of applications. Various Li metal batteries systems including Li oxygen batteries,[1,2] Li sulfur batteries,[3,4] and lithium metal batteries (LMBs) with conventional intercalation Li-ion cathodes[5,6] have been studied. However, these systems are still plagued with problems such as dendritic Li growth and poor Coulombic efficiency (CE). Recently, extensive research has been done in Li metal protection and dendrite suppression[7−12] to solve the above problems. Among these works, the development of stable organic electrolytes against Li metal is undoubtedly one of the most important research areas for enabling the long-term cycling stability of LMBs.[13,14] In a previous publication by our group,[15] a high-concentration electrolyte (HCE) composed of 4 M lithium bis(fluorosulfonyl)imide (LiFSI) salt dissolved in 1,2-dimethoxyethane (DME) was developed, which enables the long-term cycling stability of Li metal anodes with a high Li CE of 99.1%. This significant improvement in electrochemical performance compared to the conventional 1 M lithium hexafluorophosphate ($LiPF_6$)/carbonate solvent-based electrolytes is attributed to the stability of the ether solvent against Li metal, the increased solvent coordination, and the increased availability of Li^+ ions in a concentrated electrolyte.[15]

Analogous to the ether-based concentrated electrolytes, new HCEs created by mixing LiFSI salt with dimethyl carbonate (DMC) solvent at high salt concentrations were also developed and explored.[16,17] Although these HCEs enable high CE values for Li metal anodes, their practical applications are still hindered by the high electrolyte viscosity caused by the high salt concentration, the material cost, and the poor electrolyte wettability on cathodes and separators. To address these challenges, our group recently developed a new class of localized high-concentration electrolyte (LHCE)[18] by adding a diluent, bis(2,2,2-trifluoroethyl) ether (BTFE) in an HCE

Received: June 4, 2018
Accepted: July 31, 2018
Published: July 31, 2018

DOI: 10.1021/acsenergylett.8b00935
ACS Energy Lett. 2018, 3, 2059−2067

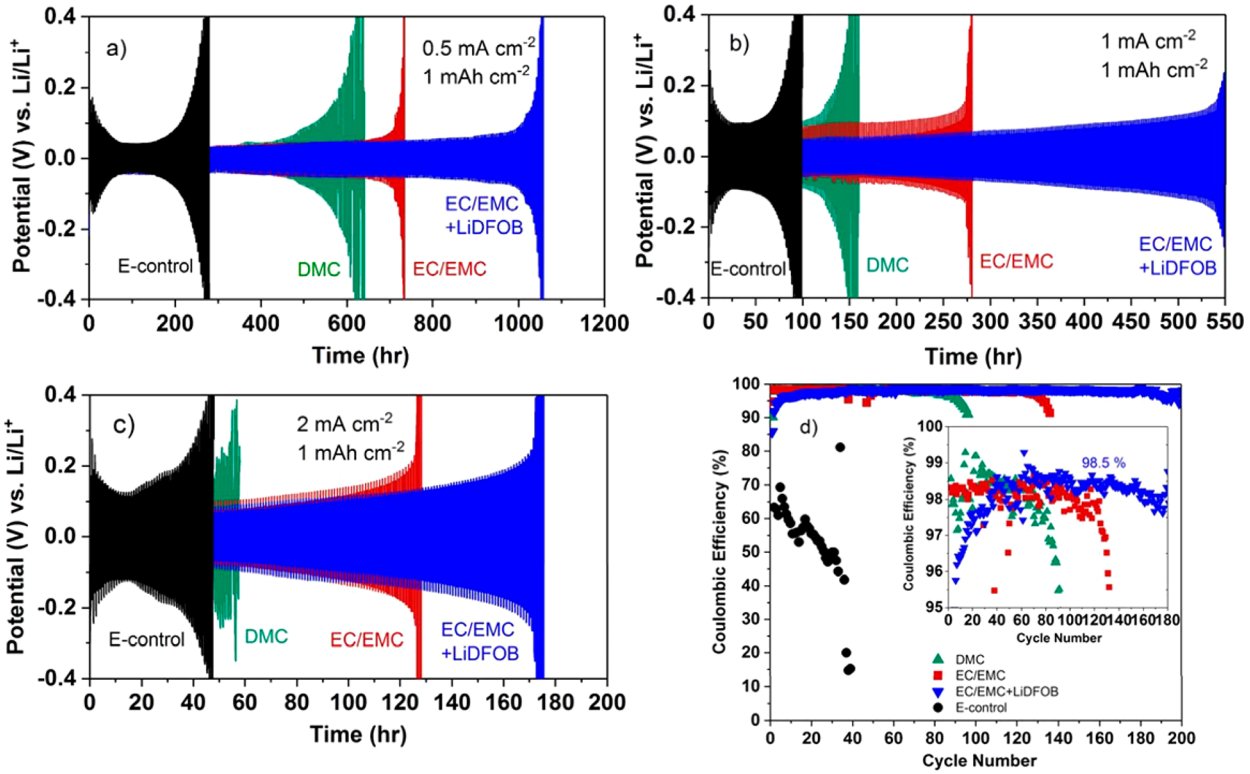

Figure 1. Galvanostatic cycling voltage profiles for Li||Li symmetrical cells at (a) 0.5, (b) 1, and (c) 2 mA cm^{-2} with a plating/stripping capacity of 1 mAh cm^{-2}. (d) Li CE from Li||Cu cells at a current density of 0.5 mA cm^{-2} and a Li plating capacity of 1 mAh cm^{-2}. The stripping cutoff voltage was 1.0 V vs Li/Li$^+$. Three LHCEs were tested: LiFSI in DMC-BTFE (green), LiFSI in EC/EMC-BTFE (red), and LiFSI in EC/EMC-BTFE with LiDFOB as an additive (blue). E-control refers to a conventional electrolyte composed of 1 M $LiPF_6$ in EC/EMC (3:7 by wt) with 2 wt % VC as an additive (black). Inset: expanded view of the CE.

composed of concentrated LiFSI salt dissolved in DMC. After dilution, the LiFSI salt concentration decreases to 1.2 M, which is comparable to the salt concentration in conventional $LiPF_6$ electrolytes. Therefore, these new LHCEs can overcome the above disadvantages (viscosity, cost, wettability) associated with HCEs. In addition, the newly developed LHCE does not sacrifice the high Li plating/stripping CE (~99%), an important characteristic of HCEs. In this Letter, we report further optimization of this new class of carbonate-based LHCEs in an effort to further improve its cycling stability with Li metal anodes and in LMBs at lean electrolyte conditions. The results reported here highlight the importance of optimizing solvents and additives in LHCEs for the development of stable organic electrolytes that can enable the practical application of rechargeable LMBs.

The previously developed LHCE[18] consisted of LiFSI, DMC, and BTFE with a salt:solvent:diluent molar ratio of 0.51:1.1:2.2. To further enhance the cycling stability of Li metal anodes in this carbonate-based LHCE, especially at lean electrolyte conditions, galvanostatic cycling tests using Li||Li symmetrical cells were first conducted with different electrolyte formulations. The main solvent DMC was changed to ethyl methyl carbonate (EMC) and an ethylene carbonate (EC)/EMC mixture, and the effect of LiDFOB as an additive was tested. For all of the LHCEs under investigation here, the molar ratio of salt:solvent:diluent was kept the same as that for the previously reported DMC-based LHCE.[18] A conventional electrolyte consisting of 1.0 M $LiPF_6$ in EC/EMC (3:7 by wt.) with 2 wt % vinylene carbonate (VC) was also tested as a control electrolyte (E-control) for comparison. In Li-ion batteries, VC was used in electrolytes to generate a high-quality solid−electrolyte interface (SEI) on the anode surface, thus improving the cycle efficiency, the high-temperature stability, and the calendar life. As can be seen from Figure 1a, at a low Li plating/stripping current density of 0.5 mA cm^{-2} and a cycling capacity of 1 mAh cm^{-2} (4 h/cycle), E-control shows poor cycling stability (~70 cycles) against Li metal, consistent with previous reports.[18] This short cycle life is mainly attributed to the poor Li plating/stripping CE of <70% as measured using Li||copper (Cu) cells (Figure 1d, black). In contrast, the previously developed LHCE of LiFSI in DMC and BTFE[18] (Figure 1a, green) shows markedly improved cycle life (~160 cycles) and stability with the Li metal anode. This is reflected also by the significant improvement of the Li CE to ~98.2% averaged over the initial 60 cycles as measured using Li||Cu cells (Figure 1d, green).

To further improve the cycling stability of Li metal in such a LHCE, the solvent DMC was first replaced with EC/EMC at a 2:8 weight ratio. This is supported by the rationale that EC tends to form a more compact SEI layer on the Li metal surface. Indeed, after replacing DMC with EC/EMC as the solvent, the cycle life of the Li||Li symmetric cell is extended to ~185 cycles (Figure 1a, red). This improvement in cycle life coming from using a dual solvent of EC/EMC is much more pronounced at higher current densities of 1 mA cm^{-2} (Figure 1b, 2 h/cycle) and 2 mA cm^{-2} (Figure 1c, 1 h/cycle). Note that there was no improvement in cycle life when DMC was replaced with EMC (Figure S1), and therefore, the positive effects are attributed to the presence of EC, which favors the formation of a more compact SEI layer.[5] LiDFOB was found

DOI: 10.1021/acsenergylett.8b00935
ACS Energy Lett. 2018, 3, 2059−2067

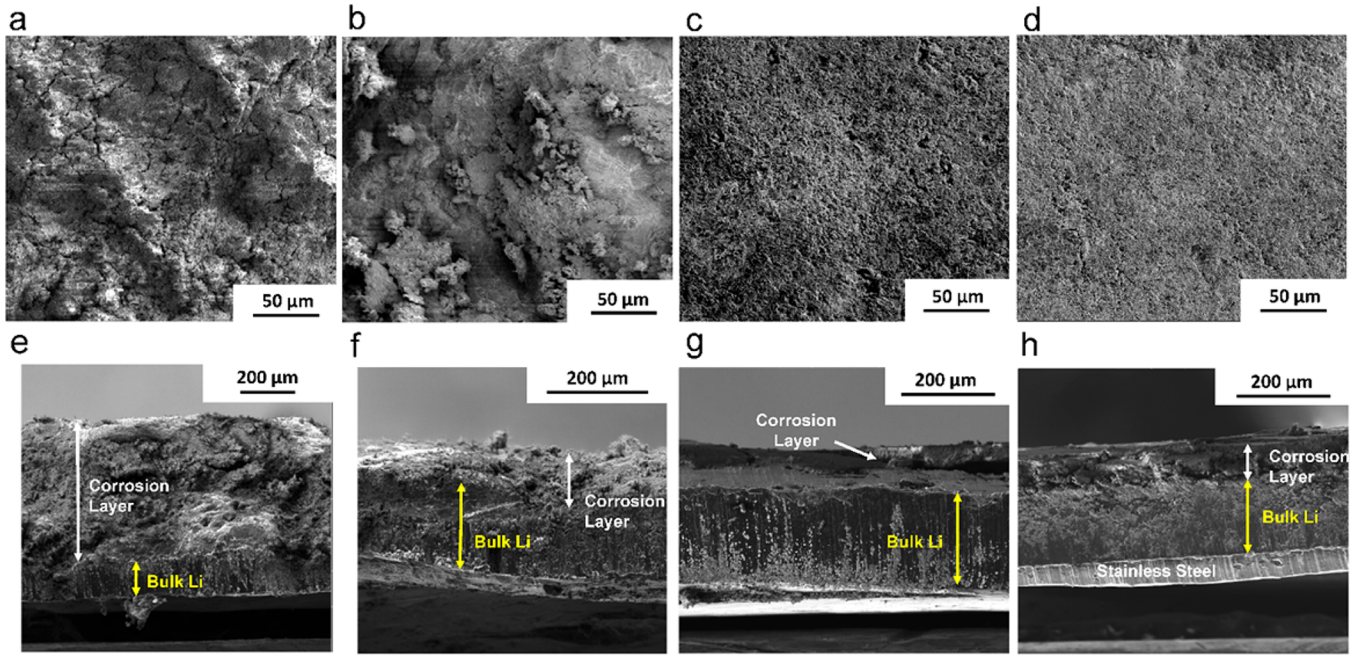

Figure 2. (a–d) Surface and (e–h) cross-sectional SEM images of Li after cycling using (a,e) E-control and three LHCEs: (b,f) LiFSI in DMC-BTFE, (c,g) LiFSI in EC/EMC-BTFE, and (d,h) LiFSI in EC/EMC-BTFE with LiDFOB as an additive. The Li electrodes were cycled at a current density of 1 mA cm^{-2} and a fixed plating/stripping capacity of 1 mAh cm^{-2} for 100 cycles.

previously to have the ability of forming a robust and conductive SEI layer by changing the SEI chemistry with oxalatoborate molecular moieties.[19] Therefore, to further improve the cycling stability of the Li metal anode, a small amount of LiDFOB (0.15 M) was added into the LHCE with EC/EMC as the solvent. As shown in Figure 1b, at a moderately high current density of 1 mA cm^{-2}, the LiDFOB-modified LHCE lasts almost 300 repeated Li plating/stripping cycles, which is approximately double the cycle life of the LHCE without LiDFOB (~140 cycles). Note that E-control lasts only about 50 cycles, and the DMC-based LHCE lasts only around 75 cycles under the same conditions (Figure 1b). In addition to the significantly improved Li metal cycling stability, the LiDFOB-modified LHCE also shows a high CE of ~98.5% (expanded view of Figure 1d) after stabilization, although the CE in the initial 30 cycles is slightly lower. This is probably due to the decomposition of LiDFOB on the Li metal anode in the early cycles,[20] which will be discussed later in detail. In summary, the above Li||Li symmetrical cell results demonstrate the synergistic effect of EC and LiDFOB in the carbonate-based LHCEs upon improving the cycling stability of Li metal anodes.

To study the morphology of Li metal after cycling in the LHCEs discussed above, surface and cross-sectional scanning electron microscopy (SEM) images of the Li metal after 100 cycles in Li||Li symmetrical cells were collected and are shown in Figure 2. For E-control, a porous surface layer with large cracks is observed after cycling (Figure 2a). The corresponding cross-sectional image (Figure 2e) shows significant corrosion of the bulk Li metal and the accumulation of a thick porous "dead" Li layer (~500 μm) due to the excessive reaction of Li with E-control. In addition, there is also noticeable expansion of Li metal: its thickness increased from the original 250 μm (before crimping) to more than 600 μm after cycling. This is not surprising given the poor Li CE of E-control reported in Figure 1d, which results in excessive corrosion layer growth. For the LHCE using DMC as the solvent, a nonuniform surface layer with mossy dendrites was also observed (Figure 2b) after cycling. The cross-sectional image (Figure 2f) shows a porous dead Li layer about 80–100 μm thick on the Li metal, and the overall thickness of Li metal and the dead Li layer is about 240 μm, which is much reduced compared to that observed using E-control. This is due to the high Li CE of the DMC-based LHCE that minimizes the side reactions between the Li metal and the electrolyte. After replacing DMC with EC/EMC, the surface morphology is drastically changed, as shown in Figure 2c. The surface now is covered by a dense SEI layer, which is attributed to the beneficial effect of EC molecule decomposition. The cross-sectional image (Figure 2g) shows that the unused bulk Li is ~200 μm thick. However, the surface layer on the Li metal shows poor adhesion and flaked off during sample preparation for SEM analysis, making the exact quantification of its thickness difficult. With further addition of LiDFOB in the LHCE with EC/EMC as the solvent, the surface layer shows better adhesion on the Li metal after cycling and the surface layer morphology becomes even more compact, as shown in Figure 2d. The unused bulk Li is about 160 μm thick, and the corrosion layer is ~80 μm thick. The increasing consumption of bulk Li after addition of LiDFOB is probably due to the slight detrimental effect of LiDFOB on the CE of initial stages of cycling, as shown in Figure 1d.

Next, the interfacial resistance of Li metal was evaluated using electrochemical impedance measurements (EIS) at different stages of symmetrical Li||Li cell cycling. The semicircle in Figure 3 of the Nyquist plots of the cells represents the interfacial resistance in the high-frequency region.[21] The values of ohmic and interfacial resistance are summarized in Table 1. After 20 cycles, all of the LHCEs show an identical ohmic resistance of about 8 Ω cm^2. The Li metal using the LHCE with DMC shows a small interfacial resistance of about 11 Ω cm^2, which is only about half of that measured using LHCEs with EC/EMC (Figure 3a). This is due to the more compact and resistive surface layer formed using the LHCEs with EC/EMC as the

DOI: 10.1021/acsenergylett.8b00935
ACS Energy Lett. 2018, 3, 2059–2067

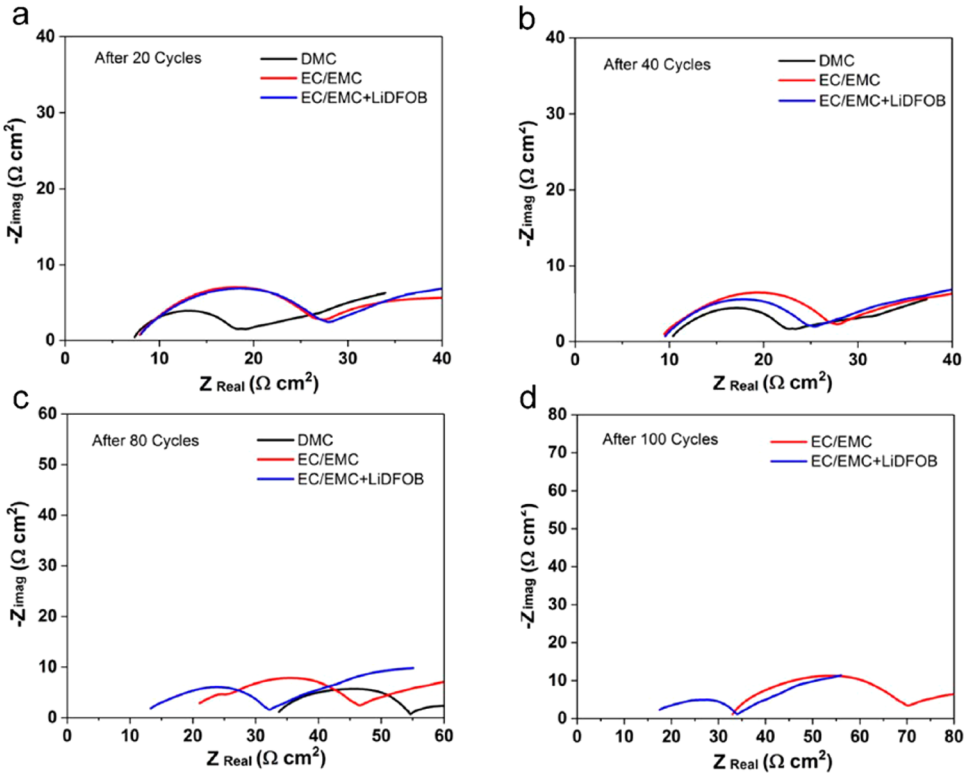

Figure 3. Nyquist plots of Li||Li symmetrical cells using three carbonate solvent-based LHCEs with BTFE as the diluent. The impedance was measured (a) after 20 cycles, (b) after 40 cycles, (c) after 80 cycles, and (d) after 100 cycles, at a current density of 2 mA cm^{-2} and a fixed plating/stripping capacity of 1 mAh cm^{-2}.

Table 1. Summary of Fitting Parameters for Nyquist Plots of Li||Li Symmetrical Cells

	20 cycles (Ω cm^{-2})		40 cycles (Ω cm^{-2})		80 cycles (Ω cm^{-2})		100 cycles (Ω cm^{-2})	
electrolyte	R_s	R_i	R_s	R_i	R_s	R_i	R_s	R_i
DMC	7.5	11	10.5	12.5	33	21.7		
EC/EMC	8	19	9.5	18.5	21	25.5	33	37.5
EC/EMC + LiDFOB	8	20	9.5	16	13.3	18.9	17.5	16.5

solvent, as supported by the SEM observations in Figure 2. After 40 cycles, there is not much change of ohmic and interfacial resistance for any of the LHCEs. However, after 80 cycles, the ohmic resistance of the DMC-based LHCE shows a large increase to 33 Ω cm^2, indicating a large consumption of electrolyte (Figure 3c). In contrast, the EC/EMC-based LHCE without LiDFOB additive shows a moderate increase in the ohmic resistance to 21 Ω cm^2, and LiDFOB addition further lowers the ohmic resistance to about 13 Ω cm^2. This suggests that a synergistic effect of EC/EMC and LiDFOB is needed to reduce electrolyte consumption during cycling. In addition, in contrast to the EC/EMC-based LHCE without LiDFOB, the interfacial resistance of the LiDFOB-modified LHCE is very stable throughout cycling, indicating a more stable and conductive SEI layer on the Li metal. For example, after 100 cycles, the EC/EMC-based LHCE without LiDFOB additive shows a further increase of ohmic and interfacial resistances to 33 and 37.5 Ω cm^2 respectively, while the LiDFOB-modified LHCE shows a much lower ohmic resistance of 17.5 Ω cm^2 and interfacial resistance of 16.5 Ω cm^2.

To further understand the effects of EC/EMC and LiDFOB on the morphology of the initial Li deposits, 1 mAh cm^{-2} of Li metal was electrochemically plated on the Cu current collector and imaged using SEM Figure 4a shows that E-control yields needle-like Li dendrites. These Li dendrites have high surface area and can lead to excessive side reactions between the Li metal and the electrolyte. For the LHCEs with DMC and EC/EMC (Figure 4b,c), the surfaces show a different morphology with granular Li and some voids among deposits. With the addition of LiDFOB, a more compact and uniform Li deposit is observed (Figure 4d), suggesting that LiDFOB can further improve the compactness of Li deposits. This is likely also responsible for the more compact SEI layer observed in Figure 2d. Figure 4e shows the elemental composition of the surface layer on the Li deposits (Figure 4a–d) collected using X-ray photoelectron spectroscopy (XPS). Compared to E-control and the LHCEs without LiDFOB, an enhancement of fluorine (F) content to 15 atom % and incorporation of 2 atom % boron (B) were found on the Li metal deposited from the LiDFOB-modified LHCE. This confirms that decomposition of LiDFOB does participate in the SEI layer formation and changes the composition of the SEI layer. The small amount of S and N found in the surface layer on the Li metal is due to the decomposition of FSI^- anions from LiFSI.[18] It has been shown that in HCEs and LHCEs FSI^- anions will decompose prior to the carbonate-based solvents.[18]

Figure 5 shows the XPS spectra of the surface of Li metal deposited using the above four electrolytes. The C 1s, F 1s, and O

DOI: 10.1021/acsenergylett.8b00935
ACS Energy Lett. 2018, 3, 2059–2067

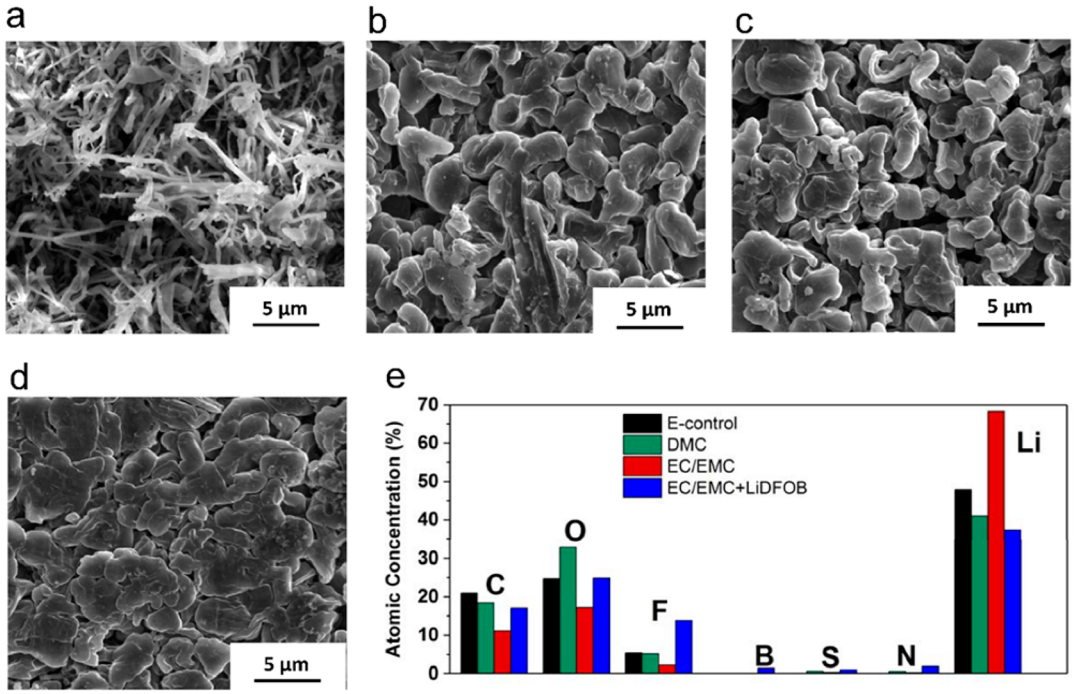

Figure 4. (a–d) SEM images of Li deposited on Cu foil at a current density of 1 mA cm^{-2} and a plating capacity of 1 mAh cm^{-2} using E-control (a) and three LHCEs: LiFSI in DMC-BTFE (b), LiFSI in EC/EMC-BTFE (c), and LiFSI in EC/EMC-BTFE with LiDFOB (d). (e) Elemental concentration of the surface layer on the Li metal deposited from E-control and three LHCEs.

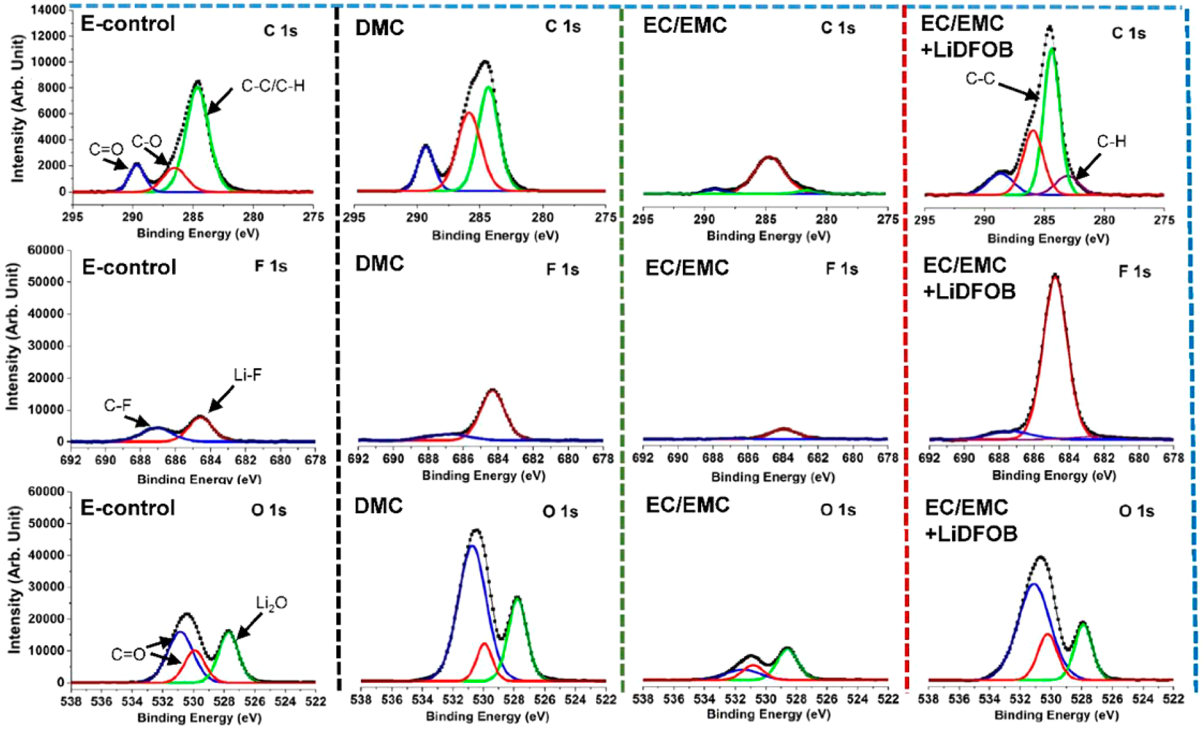

Figure 5. Narrow-scan XPS spectra of the surface layers on the electrodeposited Li metal (C 1s, F 1s, and O 1s) deposited from E-control and three carbonate solvent-based LHCEs with BTFE as the diluent. The samples were prepared by electrodepositing 1 mAh cm^{-2} Li onto Cu foil at a current density of 1 mA cm^{-2} for XPS analysis.

1s peaks have been deconvoluted. The carbonyl group (C═O) (~289.0 eV) and the ether carbon (C−O) (286 eV) have been found on the surface of Li metal deposited from the E-control and all LHCEs. The C═O and C−O groups can be attributed to the decomposition of the carbonate solvents and VC additive (for E-control). The intensities of the C═O and C−O groups in the surface layer are much lower using the LHCE with EC/EMC. This is likely due to the beneficial effect of EC, which forms a more compact SEI layer and reduces the solvent decomposition on the Li metal. With the addition of LiDFOB, more C−C and C−H compounds were detected, likely due to the decomposition of LiDFOB on the Li metal. For the F 1s

DOI: 10.1021/acsenergylett.8b00935
ACS Energy Lett. 2018, 3, 2059−2067

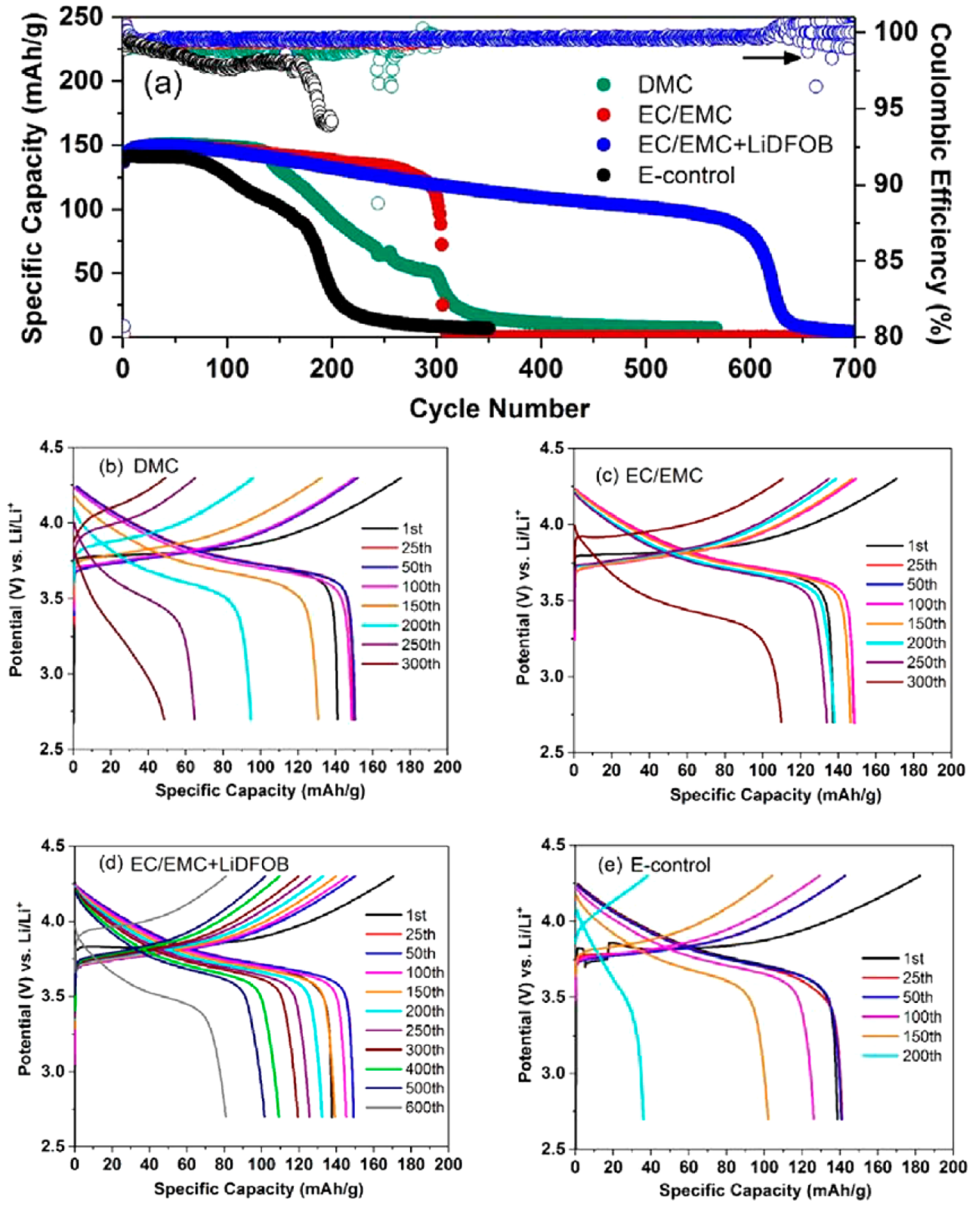

Figure 6. (a) Cycling performance of Li||NMC333 batteries using three LHCEs and E-control. (b–d) Charge/discharge voltage curves as a function of cycle number using three carbonate solvent-based LHCEs with BTFE as the diluent: LiFSI in DMC (b), LiFSI in EC/EMC (c), and LiFSI in EC/EMC with LiDFOB as an additive (d). (e) Charge/discharge voltage curves versus cycle number using a conventional electrolyte composed of 1 M $LiPF_6$ in EC/EMC (3:7 by wt) with 2 wt % VC as an additive. The Li||NMC333 batteries were cycled at 1 mA cm^{-2} for charge/discharge cycles, and the cathode areal loading was 1 mAh/cm^2.

peak, the E-control yields a mixture of organic C−F and inorganic Li−F compounds, but the F 1s peak is dominated by Li−F compounds using the LHCEs. The F element is attributed to the decomposition of LiFSI salt and BTFE diluent on the Li metal.[18] It is worth pointing out that the Li metal surface from the LiDFOB-modified LHCE is enriched with F (mainly LiF) to 15 atom %, which is much higher than that without LiDFOB (2 atom %). This high content of the LiF interphase on the Li metal has previously been found to effectively suppress Li dendrite formation and improve the interfacial stability of Li metal.[17] Therefore, enrichment of LiF on the Li metal with LiDFOB is another reason for the improved cycling stability of Li metal in the electrolyte. For the O 1s peaks, the surface layers from the four electrolytes show the same peaks corresponding to carbonyl oxygen (C═O) and lithium monoxide (Li_2O). The intensity of the C═O peak is the smallest using the LHCE with EC/EMC. When the LiDFOB is added, the intensities of the C═O and Li_2O peaks increase slightly, which can be explained by decomposition of LiDFOB and incorporation of more C═O compounds in the surface layer on the Li metal. It was reported that the electrochemical reduction of LiDFOB occurs at ∼1.6 V vs Li/Li^+[22] and results in LiF, lithium oxalate, Li_2CO_3, and cross-linked oligomeric borates.[23] In addition, the $DFOB^-$ anion can react with other components of the SEI layer such as lithium semicarbonates.[24] These reactions generate stable oligomers that are believed to make the SEI layer more elastic.[25] The improvement of SEI elasticity can suppress Li dendrite formation, and Li can deposit beneath the surface layer, providing Li metal with better protection.[25]

To further demonstrate the practicality of the LiDFOB-modified LHCE for its application in LMBs, Li||$LiNi_{1/3}Co_{1/3}$

DOI: 10.1021/acsenergylett.8b00935
ACS Energy Lett. 2018, 3, 2059−2067

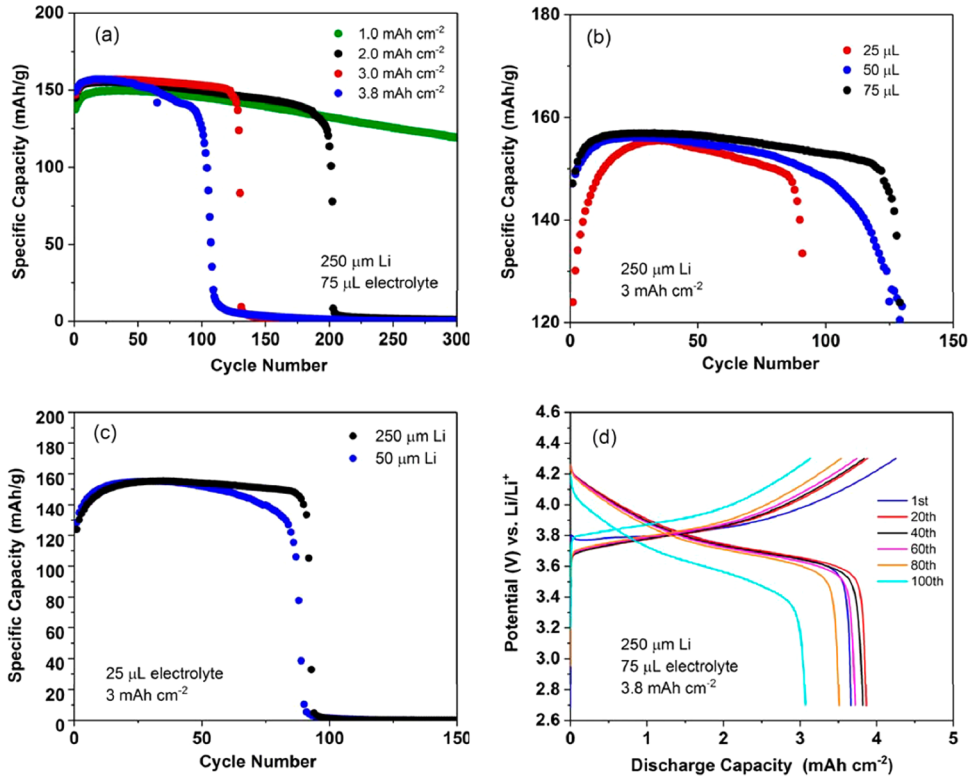

Figure 7. Charge−discharge capacity vs cycle number for Li|NMC333 batteries with (a) different cathode areal loadings, (b) different electrolyte volumes, and (c) different Li metal anode thicknesses. (d) Profiles of charge−discharge capacity vs voltage for a Li|NMC333 battery with a cathode areal loading of 3.8 mAh cm^{-2}. The Li|NMC333 batteries were all cycled with a charge/discharge current density of 1 mA cm^{-2}. The electrolyte is the LHCE consisting of 1.2 M LiFSI dissolved in EC/EMC with BTFE as the diluent and LiDFOB as an additive.

$Mn_{1/3}O_2$ (NMC333) cells were assembled with different electrolytes and their electrochemical performances were evaluated. To make a direct comparison to symmetrical cells results and facilitate data collection, the NMC333 cathode with a low areal capacity loading of 1.0 mAh cm^{-2} was used for initial tests. Figure 6a shows the specific capacity of Li|NMC333 cells at different cycle numbers using different electrolyte formulations. As expected, with the conventional $LiPF_6$-based electrolyte (E-control) under 1 mA cm^{-2} charge/discharge current densities, the Li|NMC333 battery exhibits a poor capacity retention of only 25% after 200 cycles (Figure 6a) as a result of a fast increase in cell resistance (Figure 6e) mainly related to the degradation of Li metal anode, as shown by the symmetrical cell tests in Figure 1. Because of the poor stability of the E-control with Li metal, a thick surface layer is accumulated on the Li metal after cycling (Figure 2). In comparison, the Li|NMC333 battery tested with the DMC-based LHCE shows improved cycle life and capacity retention (67% after 200 cycles). This can be attributed to the improved stability of the DMC-based LHCE with the Li metal anode. However, there is an abrupt and fast capacity fade after 140 cycles, and the battery fails after 300 cycles. Replacing DMC with EC/EMC in the LHCE enables further improvement in the capacity retention of the Li|NMC333 battery between 150 and 280 cycles, at about 96 and 85%, respectively (Figure 6c), but the battery still fails at around 300 cycles. The longest Li|NMC333 battery cycle life was achieved using the LiDFOB-modified LHCE with EC/EMC as the main solvent. In agreement with Li|Li symmetrical cell results, the addition of LiDFOB significantly improves the cycling stability of the Li metal anode (as shown by the improved Li metal morphology in Figure S2) and enables approximately 600 stable cycles of the Li|NMC333 battery. This approximately doubles the cycle life of the Li|NMC333 battery using the LHCE with EC/EMC that did not have LiDFOB added. In addition, the Li|NMC333 battery was able to maintain a reasonable specific capacity of 110 mAh g^{-1} after 400 cycles, which corresponds to 80% capacity retention (Figure 6d). This highlights the effectiveness of LiDFOB in enabling the long-term cycling stability of LMBs with LHCEs.

To further understand the factors affecting the long-term cycling stability of LMBs using the LiDFOB-modified LHCE, the cathode areal loading, the electrolyte volume, and the Li metal anode thickness were varied, and the corresponding Li|NMC333 battery performances were tested at a 1 mA cm^{-2} charge/discharge current density. Figure 7a shows the effect of the cathode areal loading on the Li|NMC333 battery cycle life. It is obvious that increasing the cathode areal loading has a detrimental effect on the Li|NMC333 battery cycle life. For example, when the areal loading is doubled from 1 to 2 mAh cm^{-2}, the cycle life decreases from ~600 cycles (Figure 6a) to 200 cycles (Figure 7a, black). Further increases in the cathode areal loading to 3.0 and 3.8 mAh cm^{-2} further reduce the cycle life to 150 and 100 cycles, respectively. Figure 7d shows the charge/discharge voltage curves for a Li|NMC333 battery with a high cathode areal loading of 3.8 mAh cm^{-2}, and the battery is able to maintain 84% of its initial capacity after 100 cycles. It has been previously reported by our group that an increase of the Li anode areal capacity (by increasing the NMC cathode areal loading) can cause severe corrosion of the Li metal anode

DOI: 10.1021/acsenergylett.8b00935
ACS Energy Lett. 2018, 3, 2059−2067

and accelerate battery capacity degradation due to a fast increase of a resistive surface degradation layer.[26] The results presented here therefore are in agreement with our previous observations. It is also observed that the discharge capacities slowly increase in the initial 10−30 cycles, which is likely due to the wetting process of the electrolyte on the cathode.

Figure 7b demonstrates the effect of another important parameter, electrolyte volume, on the cycle life of Li||NMC333 batteries. With a high cathode areal loading of 3.0 mAh cm^{-2}, increasing the electrolyte volume prolongs the Li||NMC333 cycle life. For example, increasing the electrolyte volume from 25 to 75 μL during the coin cell assembly, the battery cycle life increases from 90 to ∼130 cycles. This is a relatively small increase in cycle life considering that the electrolyte amount was tripled. This is because in LMBs the Li metal anode continuously reacts with the electrolyte during each plating/stripping cycle, which consumes electrolyte as well as Li metal, thus leading to earlier cell failure. In that sense, the more electrolyte, the longer the cycle life and better the performance of the LMB. However, the electrolyte also adds to the total weight of a battery and lowers its energy density. Therefore, it is important to develop better electrolytes that are stable with Li metal that can reach a high energy density and last long with cycling even under lean electrolyte conditions. Figure 7c shows the effect of Li metal anode thickness on the Li||NMC333 battery cycle life. Here the cathode areal loading is fixed at 3.0 mAh cm^{-2}, the electrolyte volume is fixed at 25 μL, and two Li metal anode thicknesses (50 or 250 μm) are tested. The Li||NMC333 battery cycle life is unaffected by the difference in Li metal anode thickness even when the Li anode is reduced to only 50 μm (∼2.3× excess Li relative to the cathode loading). This is not unexpected given the high Li plating/stripping CE (∼99%) of the LiDFOB-modified LHCE electrolyte, and a further reduction of the Li metal anode thickness in the Li|| NMC battery should be possible. The cycle life of the LMBs can possibly be increased by further optimizing the electrolyte composition and the charge/discharge current densities.[27]

In summary, an EC/EMC-based LHCE with LiDFOB as an additive was developed for LMBs. The addition of LiDFOB in LHCE significantly improves the cycling stability of the Li metal anode while maintaining a high Li CE of ∼99%. This improvement was also demonstrated in a Li||NMC333 battery system. With a high cathode areal loading of 3.8 mAh cm^{-2}, the Li||NMC333 battery can still maintain 84% of its initial capacity after 100 cycles even at lean electrolyte conditions, highlighting the advantages of LHCEs in high energy density LMBs. This work also provides useful information for the design of novel organic electrolytes for next-generation LMBs with high energy densities.

■ ASSOCIATED CONTENT

Supporting Information

The Supporting Information is available free of charge on the ACS Publications website at DOI: 10.1021/acsenergylett.8b00935.

Experimental methods (including materials, electrochemical tests, SEM, and XPS analysis) and additional electrochemical data and SEM images (PDF)

■ AUTHOR INFORMATION

Corresponding Authors

*E-mail: wu.xu@pnnl.gov (W.X.).
*E-mail: jiguang.zhang@pnnl.gov (J.-G.Z.).

ORCID

Shuru Chen: 0000-0003-3805-8331
Mark H. Engelhard: 0000-0002-5543-0812
Jun Liu: 0000-0001-8663-7771
Wu Xu: 0000-0002-2685-8684
Ji-Guang Zhang: 0000-0001-7343-4609

Notes

The authors declare no competing financial interest.

■ ACKNOWLEDGMENTS

This work is supported by the Assistant Secretary for Energy Efficiency and Renewable Energy, Office of Vehicle Technologies of the U.S. Department of Energy (DOE) through the Advanced Battery Materials Research (BMR) program (Battery500 Consortium) under Contract No. DE-AC02-05CH11231. The SEM and XPS measurements were conducted in the William R. Wiley Environmental Molecular Sciences Laboratory (EMSL), a national scientific user facility sponsored by DOE's Office of Biological and Environmental Research and located at Pacific Northwest National Laboratory (PNNL). PNNL is a Multiprogram National Laboratory operated by Battelle for the DOE under Contract DE-AC05-76RL01830. The LiDFOB salt was produced at the U.S. DOE Materials Engineering Research Facility (MERF) and provided by Drs. Krzysztof Z. Pupek and Trevor L. Dzwiniel of Argonne National Laboratory. The MERF Facility is fully supported by the DOE Vehicle Technologies Program within the core funding of the Applied Battery Research (ABR) for Transportation Program. The LiFSI salt was provided by Dr. Kazuhiko Murata of Nippon Shokubai Co., Ltd.

■ REFERENCES

(1) Lu, Y.-C.; Gallant, B. M.; Kwabi, D. G.; Harding, J. R.; Mitchell, R. R.; Whittingham, M. S.; Shao-Horn, Y. Lithium−Oxygen Batteries: Bridging Mechanistic Understanding and Battery Performance. *Energy Environ. Sci.* **2013**, *6* (3), 750−68.

(2) Wu, S.; Qiao, Y.; Yang, S.; Ishida, M.; He, P.; Zhou, H. Organic Hydrogen Peroxide-Driven Low Charge Potentials for High-Performance Lithium-Oxygen Batteries with Carbon Cathodes. *Nat. Commun.* **2017**, *8*, 15607.

(3) Manthiram, A.; Fu, Y.; Chung, S. H.; Zu, C.; Su, Y. S. Rechargeable Lithium-Sulfur Batteries. *Chem. Rev.* **2014**, *114* (23), 11751−87.

(4) Pang, Q.; Liang, X.; Kwok, C. Y.; Kulisch, J.; Nazar, L. F. A Comprehensive Approach toward Stable Lithium-Sulfur Batteries with High Volumetric Energy Density. *Adv. Energy Mater.* **2017**, *7* (6), 1601630.

(5) Zheng, J.; Engelhard, M. H.; Mei, D.; Jiao, S.; Polzin, B. J.; Zhang, J.-G.; Xu, W. Electrolyte Additive Enabled Fast Charging and Stable Cycling Lithium Metal Batteries. Nat. *Energy* **2017**, *2* (3), 17012.

(6) Li, X.; Zheng, J.; Ren, X.; Engelhard, M. H.; Zhao, W.; Li, Q.; Zhang, J.-G.; Xu, W. Dendrite-Free and Performance-Enhanced Lithium Metal Batteries through Optimizing Solvent Compositions and Adding Combinational Additives. *Adv. Energy Mater.* **2018**, *8*, 1703022.

(7) Lee, H.; Ren, X.; Niu, C.; Yu, L.; Engelhard, M.; Cho, I.; Ryou, M.-H.; Jin, H. S.; Kim, H.-T.; Liu, J.; Xu, W.; Zhang, J. G. Suppressing Lithium Dendrite Growth by Metallic Coating on a Separator. *Adv. Funct. Mater.* **2017**, *27* (45), 1704391.

(8) Yun, Q.; He, Y. B.; Lv, W.; Zhao, Y.; Li, B.; Kang, F.; Yang, Q. H. Chemical Dealloying Derived 3D Porous Current Collector for Li Metal Anodes. *Adv. Mater.* **2016**, *28* (32), 6932−9.

DOI: 10.1021/acsenergylett.8b00935
ACS Energy Lett. 2018, 3, 2059−2067

(9) Ye, H.; Xin, S.; Yin, Y.-X.; Guo, Y.-G. Advanced Porous Carbon Materials for High-Efficient Lithium Metal Anodes. *Adv. Energy Mater.* **2017**, *7* (23), 1700530.
(10) Yu, L.; Canfield, N. L.; Chen, S.; Lee, H.; Ren, X.; Engelhard, M. H.; Li, Q.; Liu, J.; Xu, W.; Zhang, J.-G. Enhanced Stability of Lithium Metal Anode by using a 3D Porous Nickel Substrate. *ChemElectroChem* **2018**, *5* (5), 761−769.
(11) Markevich, E.; Salitra, G.; Chesneau, F.; Schmidt, M.; Aurbach, D. Very Stable Lithium Metal Stripping−Plating at a High Rate and High Areal Capacity in Fluoroethylene Carbonate-Based Organic Electrolyte Solution. *ACS Energy Lett.* **2017**, *2* (6), 1321−1326.
(12) Yan, C.; Cheng, X. B.; Tian, Y.; Chen, X.; Zhang, X. Q.; Li, W. J.; Huang, J. Q.; Zhang, Q. Dual-Layered Film Protected Lithium Metal Anode to Enable Dendrite-Free Lithium Deposition. *Adv. Mater.* **2018**, *30* (25), 1707629.
(13) Zhang, X. Q.; Chen, X.; Cheng, X. B.; Li, B. Q.; Shen, X.; Yan, C.; Huang, J. Q.; Zhang, Q. Highly Stable Lithium Metal Batteries Enabled by Regulating the Solvation of Lithium Ions in Nonaqueous Electrolytes. *Angew. Chem., Int. Ed.* **2018**, *57* (19), 5301−5305.
(14) Zhang, X. Q.; Cheng, X. B.; Chen, X.; Yan, C.; Zhang, Q. Fluoroethylene Carbonate Additives to Render Uniform Li Deposits in Lithium Metal Batteries. *Adv. Funct. Mater.* **2017**, *27* (10), 1605989.
(15) Qian, J.; Henderson, W. A.; Xu, W.; Bhattacharya, P.; Engelhard, M.; Borodin, O.; Zhang, J. G. High Rate and Stable Cycling of Lithium Metal Anode. *Nat. Commun.* **2015**, *6*, 6362.
(16) Wang, J.; Yamada, Y.; Sodeyama, K.; Chiang, C. H.; Tateyama, Y.; Yamada, A. Superconcentrated Electrolytes for a High-Voltage Lithium-Ion Battery. *Nat. Commun.* **2016**, *7*, 12032.
(17) Fan, X.; Chen, L.; Ji, X.; Deng, T.; Hou, S.; Chen, J.; Zheng, J.; Wang, F.; Jiang, J.; Xu, K.; Wang, C. Highly Fluorinated Interphases Enable High-Voltage Li-Metal Batteries. *Chem.* **2018**, *4* (1), 174−185.
(18) Chen, S.; Zheng, J.; Mei, D.; Han, K. S.; Engelhard, M. H.; Zhao, W.; Xu, W.; Liu, J.; Zhang, J. G. Lithium-Metal Batteries: High-Voltage Lithium-Metal Batteries Enabled by Localized High-Concentration Electrolytes. *Adv. Mater.* **2018**, *30*, 1870144.
(19) Zhang, S. S. Electrochemical Study of the Formation of a Solid Electrolyte Interface on Graphite in a $LiBC_2O_4F_2$-based Electrolyte. *J. Power Sources* **2007**, *163* (2), 713−718.
(20) Schedlbauer, T.; Krüger, S.; Schmitz, R.; Schmitz, R. W.; Schreiner, C.; Gores, H. J.; Passerini, S.; Winter, M. Lithium Difluoro(oxalato)borate: A Promising Salt for Lithium Metal Based Secondary Batteries? *Electrochim. Acta* **2013**, *92*, 102−107.
(21) Bieker, G.; Winter, M.; Bieker, P. Electrochemical In Situ Investigations of SEI and Dendrite Formation on the Lithium Metal Anode. *Phys. Chem. Chem. Phys.* **2015**, *17* (14), 8670−9.
(22) Xia, L.; Lee, S. X.; Jiang, Y. B.; Xia, Y. G.; Chen, G. Z.; Liu, Z. P. Fluorinated Electrolytes for Li-Ion Batteries: The Lithium Difluoro-(oxalato)borate Additive for Stabilizing the Solid Electrolyte Interphase. *ACS Omega* **2017**, *2* (12), 8741−8750.
(23) Parimalam, B. S.; Lucht, B. L. Reduction Reactions of Electrolyte Salts for Lithium Ion Batteries: $LiPF_6$, $LiBF_4$, LiDFOB, LiBOB, and LiTFSI. *J. Electrochem. Soc.* **2018**, *165* (2), A251−A255.
(24) Zhang, S. S. An Unique Lithium Salt for the Improved Electrolyte of Li-ion Battery. *Electrochem. Commun.* **2006**, *8*, 1423.
(25) Aurbach, D.; Markovsky, B.; Levi, M. D.; Levi, E.; Schechter, A.; Moshkovich, M.; Cohen, Y. New Insights into the Interactions Between Electrode Materials and Electrolyte Solutions for Advanced Nonaqueous Batteries. *J. Power Sources* **1999**, *81-82*, 95.
(26) Jiao, S.; Zheng, J.; Li, Q.; Li, X.; Engelhard, M. H.; Cao, R.; Zhang, J.-G.; Xu, W. Behavior of Lithium Metal Anodes under Various Capacity Utilization and High Current Density in Lithium Metal Batteries. *Joule* **2018**, *2* (1), 110−124.
(27) Zheng, J.; Yan, P.; Mei, D.; Engelhard, M. H.; Cartmell, S. S.; Polzin, B. J.; Wang, C.; Zhang, J.-G.; Xu, W. Highly Stable Operation of Lithium Metal Batteries Enabled by the Formation of a Transient High-Concentration Electrolyte Layer. *Adv. Energy Mater.* **2016**, *6* (8), 1502151.

DOI: 10.1021/acsenergylett.8b00935
ACS Energy Lett. 2018, 3, 2059−2067